

# Investigating the unification of LOFAR-detected powerful AGN in the Boötes field

Leah K. Morabito,<sup>1,2\*</sup> W. L. Williams,<sup>3</sup> Kenneth J. Duncan,<sup>1</sup> H. J. A. Röttgering,<sup>1</sup> George Miley,<sup>1</sup> Aayush Saxena,<sup>1</sup> Peter Barthel,<sup>4</sup> P. N. Best,<sup>5</sup> M. Bruggen,<sup>6</sup> G. Brunetti,<sup>7</sup> K. T. Chyży,<sup>8</sup> D. Engels,<sup>6</sup> M. J. Hardcastle,<sup>3</sup> J. J. Harwood,<sup>9</sup> Matt J. Jarvis,<sup>2,10</sup> E. K. Mahony,<sup>11,12</sup> I. Prandoni,<sup>7</sup> T. W. Shimwell,<sup>1</sup> A. Shulevski<sup>9</sup> and C. Tasse<sup>13,14</sup>

<sup>1</sup>Leiden Observatory, Leiden University, PO Box 9513, NL-2300 RA Leiden, the Netherlands

<sup>2</sup>Astrophysics, University of Oxford, Denys Wilkinson Building, Keble Road, Oxford OX1 3RH, UK

<sup>3</sup>Centre for Astrophysics Research, School of Physics, Astronomy and Mathematics, University of Hertfordshire, College Lane, Hatfield AL10 9AB, UK

<sup>4</sup>Kapteyn Astronomical Institute, University of Groningen, PO Box 800, NL-9700 AV Groningen, the Netherlands

<sup>5</sup>SUPA, Institute for Astronomy, Royal Observatory, Blackford Hill, Edinburgh EH9 3HJ, UK

<sup>6</sup>Universität Hamburg, Hamburger Sternwarte, Gojenbergsweg 112, D-21029 Hamburg, Germany

<sup>7</sup>INAF – Istituto di Radioastronomia, via P. Gobetti 101, I-40129 Bologna, Italy

<sup>8</sup>Astronomical Observatory, Jagiellonian University, ul. Orła 171, PL-30-244 Kraków, Poland

<sup>9</sup>ASTRON, The Netherlands Institute for Radio Astronomy, Postbus 2, NL-7990 AA Dwingeloo, the Netherlands

<sup>10</sup>Department of Physics, University of the Western Cape, Cape Town 7535, South Africa

<sup>11</sup>Sydney Institute for Astronomy, School of Physics A28, The University of Sydney, NSW 2006, Australia

<sup>12</sup>ARC Centre of Excellence for All-Sky Astrophysics (CAASTRO), Australia

<sup>13</sup>GEPI, Observatoire de Paris, CNRS, Université Paris Diderot, 5 place Jules Janssen, F-92190 Meudon, France

<sup>14</sup>Department of Physics and Electronics, Rhodes University, PO Box 94, Grahamstown 6140, South Africa

Accepted 2017 April 19. Received 2017 March 31; in original form 2017 January 5

## ABSTRACT

Low radio frequency surveys are important for testing unified models of radio-loud quasars and radio galaxies. Intrinsically similar sources that are randomly oriented on the sky will have different projected linear sizes. Measuring the projected linear sizes of these sources provides an indication of their orientation. Steep-spectrum isotropic radio emission allows for orientation-free sample selection at low radio frequencies. We use a new radio survey of the Boötes field at 150 MHz made with the Low-Frequency Array (LOFAR) to select a sample of radio sources. We identify 60 radio sources with powers  $P > 10^{25.5} \text{ W Hz}^{-1}$  at 150 MHz using cross-matched multiwavelength information from the AGN and Galaxy Evolution Survey, which provides spectroscopic redshifts and photometric identification of 16 quasars and 44 radio galaxies. When considering the radio spectral slope only, we find that radio sources with steep spectra have projected linear sizes that are on average  $4.4 \pm 1.4$  larger than those with flat spectra. The projected linear sizes of radio galaxies are on average  $3.1 \pm 1.0$  larger than those of quasars ( $2.0 \pm 0.3$  after correcting for redshift evolution). Combining these results with three previous surveys, we find that the projected linear sizes of radio galaxies and quasars depend on redshift but not on power. The projected linear size ratio does not correlate with either parameter. The LOFAR data are consistent within the uncertainties with theoretical predictions of the correlation between the quasar fraction and linear size ratio, based on an orientation-based unification scheme.

**Key words:** galaxies: active – galaxies: jets – radio continuum: galaxies.

## 1 INTRODUCTION

Active galactic nuclei (AGNs) produce high nuclear luminosities that cannot be explained by star formation alone. They are believed to be powered by accretion on to a central supermassive black hole.

\* E-mail: [leah.morabito@physics.ox.ac.uk](mailto:leah.morabito@physics.ox.ac.uk)

AGNs can exhibit a wide variety of observational characteristics, including high luminosities in the optical and near-infrared (IR), strong emission lines from ionized gas and high mid-IR luminosities. AGNs that have strong emission lines in their spectra are classified as type 1 or type 2 based on whether their emission lines are broad (typically  $>2000 \text{ km s}^{-1}$ ) or narrow ( $<2000 \text{ km s}^{-1}$ ). Type 1 AGNs show broad and narrow emission lines while type 2 AGNs show only narrow emission lines.

Under the current unification paradigm (Antonucci 1993; Urry & Padovani 1995), type 1 and type 2 AGNs exhibit different observed characteristics due to the presence of a dusty structure or torus that will obscure the accretion disc and broad-line region depending on viewing angle to the AGN. Those AGNs that exhibit broad emission lines were historically associated with bright optical point sources, leading to the term ‘quasi-stellar object’ or quasar. Type 1 AGNs are oriented such that the accretion disc and broad-line emission regions are seen directly without obscuration from the torus. They include radio-loud and radio-quiet quasars as well as type 1 Seyfert galaxies. Type 2 AGNs are oriented such that the broad-line emission region and accretion disc are obscured by the dusty torus and not directly visible.

About 10 per cent of AGNs exhibit extended powerful radio emission in the form of jets that reach far beyond the host galaxy and can provide an indication of orientation. Low radio frequency surveys are important for selecting these objects in an orientation-independent way, as high-frequency surveys are biased towards core-dominated flat-spectrum objects where the jets are pointed towards the observer. The radio fluxes of radio-loud AGNs at low frequencies are dominated by emission from the lobes, rather than the hotspots and/or jets, thus minimizing any possible orientation-based effects like Doppler boosting. These radio-loud AGNs comprise two populations, believed to be powered by different accretion modes. Radio galaxies that exhibit strong emission lines in the optical regime and evidence of a torus in the mid-IR are referred to as high-excitation radio galaxies (HERGs). HERGs can be either type 1 or type 2 AGNs. The AGNs in HERGs are thought to be powered via a geometrically thin and optically thick accretion disc (Shakura & Sunyaev 1973), which is believed to be fed by large central repositories of cold gas (e.g. Larson 2010). This has led to the name ‘cold-mode’ accretion (Hardcastle, Evans & Croston 2007).

The second type of radio-loud AGNs lacks the strong emission lines seen in HERGs and termed low-excitation radio galaxies (LERGs). They also lack evidence for a dusty torus (e.g. Whyson & Antonucci 2004; Ogle, Whyson & Antonucci 2006; Tasse et al. 2008; van der Wolk et al. 2010) and for a full accretion disc (e.g. Evans et al. 2006; Hardcastle, Evans & Croston 2006). LERGs are thought to be powered by ‘hot-mode’ accretion processes, where hot gas is accreted via advection-dominated accretion or radiatively inefficient accretion flows (e.g. Narayan & Yi 1994; Quataert 2001; Ho 2008). For these reasons, the non-radio spectral energy distributions of LERGs are not expected to show strong orientation effects. Best & Heckman (2012) showed that LERGs dominate the population of low-power ( $P_{1.4\text{GHz}} \lesssim 10^{25} \text{ W Hz}^{-1}$ ) sources at least in the local Universe and tend to be associated with edge-dimmed radio jets of Fanaroff–Riley Class I objects (FR I; Fanaroff & Riley 1974), although this is not a hard division with one-to-one mapping.

The discovery of superluminal motion in radio jets was strong evidence that some radio sources have their jets aligned close (within  $\sim 15^\circ$ ) to the line of sight (Barthel et al. 1989). Radio sources with beamed flat-spectrum cores consistent with superluminal motion should have smaller projected sizes on average than steep-spectrum

radio sources with jets oriented further from the line of sight. This scenario can be extended to HERGs, where the difference in orientation is indicated by whether or not the line of sight reveals emission from the accretion disc. Radio galaxies are those objects in which the obscuring torus is viewed edge-on and the accretion disc emission is hidden, while quasars are viewed with a direct line of sight to the accretion disc. Radio galaxies will therefore have radio jets preferentially oriented closer to the plane of the sky, while quasars will have radio jets closer to the line of sight.

The radio orientation is clearly linked to the orientation of the torus/accretion disc, as shown by the detection of significant optical polarization aligned with the radio jets in nearby galaxies (e.g. Antonucci 1982; Schmidt & Smith 2000). The observed properties of strong line AGNs (HERGs) at wavelengths other than radio are consistent with orientation schemes, mostly due to the presence of a dusty obscuring structure. For example, the presence of broad lines in polarized light of type 1 AGNs (narrow-line galaxies) is powerful evidence for hidden quasars whose light is reflected outside of the obscuring structure (e.g. Antonucci 1984; Ogle et al. 1997; Cohen et al. 1999).

Barthel (1989) used the Third Cambridge Catalogue of Radio Sources (3CRR) survey of radio sources at 178 MHz (Laing, Riley & Longair 1983) to study the projected linear sizes for 42 radio sources with optical identifications and spectroscopic redshifts for the range  $0.5 \leq z \leq 1$ . Barthel found that there was a division between radio sources: those associated with quasars were on average 2.2 times smaller than the other radio sources. The 3CRR sample is now 100 per cent spectroscopically complete, and classifications based on emission line ratios have been used to identify HERGs (which are expected to show orientation effects) and LERGs (which are not expected to show orientation effects). The high limiting flux density of the survey means that only 13 per cent have been found to be LERGs (Willott et al. 1999) and therefore were not a large contaminant at the redshift range used by Barthel (1989).

Follow-up studies have tended to confuse the issue. A reassessment of the 3CRR sample by Singal (2014) found systematically larger sizes of radio galaxies compared to radio-loud quasars only for redshifts above 0.5. For lower redshifts, radio galaxies were on average larger than radio-loud quasars but only when their cumulative linear sizes were above  $\sim 400 \text{ kpc}$ . Singal & Singh (2013) also studied the linear sizes of a 98 per cent spectroscopically complete sample selected at 408 MHz (Best, Röttgering & Lehnert 1999), finding that only at redshifts larger than 1 were the linear sizes of radio galaxies systematically larger than those of quasars. The authors made no attempt to remove LERGs from the sample but argued that they would have to be a large part of the sample to change the results. However, these studies still cover only a small part of the power–redshift ( $P-z$ ) diagram, and it is important to collect more information to investigate this further.

A further motivation for larger studies comes from DiPompeo et al. (2013). The authors use Monte Carlo modelling to show that intrinsic size distributions and the intrinsic angle of division between radio galaxies and quasars,  $\theta_c$ , can influence the results. While they do not consider in their models that  $\theta_c$  should correlate directly with the linear size ratio, they estimate that for  $\theta_c = 45^\circ$  (Barthel 1989, found  $\theta_c = 44.4^\circ$ ) several hundred sources are necessary for a significant difference in the cumulative measured sizes. Their comparison to other data sets that seem to contradict orientation-only unification schemes (Singal & Singh 2013, and an unpublished study) does not consider observational biases (e.g. classification of LERGs/HERGs) that might be present in the data. Here we try to overcome these biases by using a new low-frequency selected

sample and by combining and considering all available data for a broader test of orientation-based unification schemes.

In this study, we use a new low-frequency radio survey of the Boötes field (Williams et al. 2016) with the Low-Frequency Array (LOFAR; van Haarlem et al. 2013) to investigate the unification of radio sources in two ways. First, we look at the difference in projected linear sizes of flat- and steep-spectrum sources, without any classification from other wavelengths. Second, we investigate the difference in projected linear sizes of cold-mode accretion sources by splitting our sample into *quasars* and *radio galaxies* using available multiwavelength data including spectroscopic redshifts and quasar classifications from the AGN and Galaxy Evolution Survey (AGES; Kochanek et al. 2012). It is difficult to measure properly the sizes of edge-dimmed FR I sources, and we make a power cut at  $P_{150\text{MHz}} > 10^{25.5} \text{ W Hz}^{-1}$  to exclude these sources and star-forming galaxies at lower powers (Saxena, Röttgering & Rigby 2017) as much as possible. This means our sample is likely to be dominated by HERGs, although it is difficult to determine this based on broad-band photometry alone (chap. 5 of Janssen 2017).

The new LOFAR catalogue contains over 6000 radio sources to an rms depth of  $\sim 120\text{--}150 \mu\text{Jy beam}^{-1}$  at 150 MHz. While previous samples used to test orientation-based unification probed high-luminosity sources over large areas of the sky, the deep LOFAR data probe a large number of fainter sources over a smaller area. This adds a substantial number of sources to the  $P$ - $z$  diagram at lower powers compared to previous samples, especially for higher redshifts.

Section 2 first describes the LOFAR survey, the multiwavelength data and the selection of quasars and radio galaxies. Results from the LOFAR survey are presented in Section 3. The LOFAR results combined with two previous samples are presented in Section 4. Discussion and conclusions follow in Sections 5 and 6. Throughout the paper we assume a  $\Lambda$  cold dark matter ( $\Lambda$ CDM) concordance cosmology with  $H_0 = 67.8 \text{ km s}^{-1} \text{ Mpc}^{-1}$ ,  $\Omega_m = 0.308$  and  $\Omega_\Lambda = 0.692$ , consistent with Planck Collaboration XIII (2016). Spectral index is defined as  $\alpha$  with flux density  $S \propto \nu^\alpha$ . Throughout the paper, all ‘linear sizes’ referred to are projected linear sizes.

## 2 THE BOÖTES FIELD DATA

In this section, we present the construction of our radio galaxy and quasar samples. We start by describing the new LOFAR Boötes survey, the cross-matching of radio and pre-existing multiwavelength data and how we select our sample. Finally, we discuss possible biases in our sample selection.

### 2.1 LOFAR Boötes survey

The catalogue from Williams et al. (2016) contains a total of 6267 radio sources within  $19 \text{ deg}^2$ . The rms varies over the field of view, and sources with peak fluxes exceeding a threshold of  $5\sigma$  above the local rms were included in the final catalogue. The rms is less than  $120 \mu\text{Jy beam}^{-1}$  at the centre and more than 50 per cent of the field of view has rms noise less than  $180 \mu\text{Jy beam}^{-1}$ . The average rms noise at the edges of the optical coverage is approximately  $150 \mu\text{Jy beam}^{-1}$ . The resolution of the LOFAR image is  $5.6 \times 7.4 \text{ arcsec}^2$ , with average positional accuracy of  $\sim 0.4 \text{ arcsec}$ .

The sources in the catalogue are divided into classes based on radio morphology. Here we consider only single sources or extended sources with a radio core (VClass 1/11) and double sources with no obvious radio core (VClass 2/21). These will be mostly FR II, FR I or single-component sources. The other morphological classifications

make up only 0.1 per cent of the catalogue. These sources have either diffuse or complex morphologies and not expected to be the radio sources in which we are interested.

### 2.2 Adding in multiwavelength data

To carry out this study, we require two pieces of information: spectroscopic redshifts, and the ability to split our LOFAR-detected radio-loud AGNs into quasars and radio galaxies. The spectroscopic redshifts are necessary to calculate precise linear sizes of radio sources and avoid propagating large and uncertain errors due to photometric redshifts. The quasar/radio galaxy classifications are necessary to divide the sources into the desired samples. Ideally, we would target all LOFAR-detected sources to acquire both spectroscopic redshift and enough information to distinguish spectroscopically between radio galaxies (narrow-line AGNs) and quasars (broad- and narrow-line AGNs). A dedicated survey with the William Herschel Telescope Enhanced Area Velocity Explorer (WEAVE) that goes online in 2018 (WEAVE-LOFAR; Smith 2016) will provide spectroscopic redshifts and possibly emission line ratios for LOFAR-detected sources within the next few years. As these data do not exist yet, we use available multiwavelength information.

The NOAO Deep Wide-Field Survey (NDWFS; Jannuzi & Dey 1999) covers  $9 \text{ deg}^2$  of the Boötes field with deep optical to near-IR photometric data ( $B_w, R, I, J, K$ ). Ancillary data at longer wavelengths cover the near- to mid-IR [Infrared Array Camera (IRAC) 3.6, 4.5, 5.8 and  $8.0 \mu\text{m}$ , and Multiband Imaging Photometer for *Spitzer* (MIPS)  $24 \mu\text{m}$ ]. A multiwavelength catalogue of these data, based on Brown et al. (2007, 2008), was used for the optical identification of radio sources, described in Williams et al. (2017). Within the NDWFS sky coverage, there are 3894 LOFAR-detected sources; of these, 76 per cent, or 2971 sources, have an optical counterpart.

The AGES (Kochanek et al. 2012) is based on the NDWFS data, as well as complementary ultraviolet, radio and X-ray data. The NDWFS contains more than 2 million optical sources, and Kochanek et al. (2012, hereafter K12) aimed to provide a statistically robust sample of normal galaxies via random sparse sampling, and a complete sample of targeted AGN candidates (selected from the combination of multiwavelength photometric data). These samples were targeted for spectroscopic redshift measurements using the Hectospec instrument on the Multiple Mirror Telescope (MMT). From 8977 AGN candidates, spectra were taken for 7102 and redshifts obtained for 4764 (after excluding Galactic stars, which made up 9 per cent of successful redshifts). Measured spectroscopic redshifts are therefore available for  $\sim 53$  per cent of AGN candidates in AGES. In total, there are spectroscopic redshifts for 18 163 galaxies (to  $I = 20 \text{ mag}$ ) and 4764 AGN candidates (to  $I = 22.5 \text{ mag}$ ). There are 1106 LOFAR-detected sources with optical counterparts that have spectroscopic redshifts in AGES.

### 2.3 Selecting the final samples

The way we select our final sample is as follows.

- (i) Select all LOFAR-detected sources with optical counterparts.
- (ii) Select only optical counterparts with spectroscopic redshifts from AGES.
- (iii) Use the K12 classification codes to identify quasars.
- (iv) Those sources not identified as quasars are considered to be radio galaxies.

(v) Check that all radio galaxies satisfy the mid-IR 24  $\mu\text{m}$  criteria, which indicates the presence of a dusty torus (and are therefore not likely to be LERGs).

(vi) Make a radio power cut of  $P \geq 10^{25.5} \text{ W Hz}^{-1}$  to exclude FR I and star-forming galaxies.

For all sources with spectroscopic information, K12 provide classification codes. There are five AGN classifications that rely on different photometric bands of the multiwavelength data (described in detail in K12). AGNs can be selected based on compact, bright optical morphology, near-IR colour selections (based on Stern et al. 2005), bright mid-IR luminosities, the presence of X-ray point sources and radio detections at 1.4 GHz. A small fraction of sources that were initially part of the normal galaxies sample are also identified as AGNs in the catalogue. We use these AGN classifications to identify quasars as those objects satisfying the optical and/or near-IR colour criteria (in line with above), and the rest of our sample is therefore defined as radio galaxies. We check that all of the radio galaxies in our final sample satisfy the mid-IR 24  $\mu\text{m}$  criteria (as above), which indicates the presence of a dusty torus (and these sources are therefore not likely to be LERGs).

For this study, we are interested only in powerful FR II sources. The last step in constructing our sample is to make a power cut at  $10^{25.5} \text{ W Hz}^{-1}$  to remove the lower power sources that are either star-forming galaxies or more likely to have FR I morphology (since FR I sources are dimmer at the edges, their linear sizes are not well defined). This cut is suggested as appropriate by previous data and theoretical models (Saxena et al., 2017). To test whether we can divide the sample into higher power bins, we construct radio luminosity functions (RLFs) following the grid-based method in Rigby et al. (2015). A comparison of the RLFs for our sample with model RLFs from Rigby et al. (2011) shows that the observed RLF for the LOFAR sample with  $P_{150\text{MHz}} \geq 10^{25.5} \text{ W Hz}^{-1}$  has similar behaviour to the model RLF, i.e. the trends in space density are the same, suggesting that the sample is representative of the entire population. Introducing higher power cuts in the LOFAR sample changes the observed RLF, as the space density of radio sources in the LOFAR sample drops off sharply above  $z = 2$  with higher power cuts. We therefore do not consider higher power cuts in this analysis. The final sample comprises 44 radio galaxies and 16 quasars, and their properties are listed in Table 1.

Not all sources are resolved by this low-frequency survey, as identified by Williams et al. (2016). 21 sources are unambiguously detected as having edge-brightened lobes typical of FR II sources, 25 sources do not have individually resolved components but are clearly extended and 14 sources are considered to be truly unresolved (point sources). Many of the unresolved sources have extended, edge-bright morphology that suggests they would be identified as FR II sources if imaged at higher resolution. Eight of the unresolved sources are quasars. In the case of the unresolved sources, we use the deconvolved major axis as the largest angular size. The power cut makes it highly likely they are FR II-type sources, and we leave them in the sample.

## 2.4 Investigating possible biases in the sample selection

We identify quasars (and thus radio galaxies) based on the photometric information in AGES. The complicated AGES sample selection, and the fact that it changed several times over the duration of the survey, means it is not straightforward to estimate the completeness of our final sample. Nevertheless, we investigate several aspects to identify any biases that might exist in our final sample.

First, we select all sources in AGES, regardless of LOFAR detections, and identify sources with identical criteria to selecting the radio galaxy and quasar samples. This allows us to see if the selection criteria preferentially favour successful spectroscopic redshifts for one sample relative to the other. We find similar spectroscopic completeness of both samples as a function of both (i)  $K_s$ -band magnitude and (ii)  $I$ -band magnitude. This implies that we are not biased towards one sample over the other because of apparent brightness. However, the magnitude cut itself may introduce a bias in the quasar fraction if quasars are intrinsically brighter in the  $I$  band than radio galaxies. Powerful radio galaxies are often found in massive, red galaxies that will be harder to detect at redshifts  $\gtrsim 1$ , which could artificially increase the quasar fraction at higher redshifts.

Next, we compare the distributions of spectroscopic redshifts for the two samples. The distributions have similar lognormal behaviour, as expected from a flux-limited survey, with fewer objects from both samples found at higher redshifts. For the redshift range  $0.4 \lesssim z \lesssim 1$ , we find a slight dip in the quasar redshift distribution. To investigate this, we compare the spectroscopic redshift distribution for the quasar sample to photometric redshifts for the same sample. The photometric redshifts are from Duncan et al. (in preparation) and are combined from estimates produced using EAZY (Brammer, van Dokkum & Coppi 2008) and three different sets of templates. These template sets are (a) the default set of EAZY templates, (b) the Spitzer Wide-Area Infrared Extragalactic Survey (SWIRE) template library from Polletta et al. (2007) and (c) the ‘Atlas of Galaxy SEDs’ from Brown et al. (2014). The final photometric redshifts are a hierarchical Bayesian combination of the results of the individual photometric redshift catalogues. The photometric redshift distribution shows the expected lognormal behaviour and does not show the dip that is seen in the spectroscopic redshift distribution. The comparison indicates that the spectroscopic completeness falls from about 48 to 40 per cent in this redshift range. The loss of sources in this redshift range is only about one-tenth of the entire spectroscopic quasar sample, and this is not likely to strongly bias our general results. The comparison of spectroscopic and photometric redshift distributions for the quasar sample is shown in the left-hand panel of Fig. 1.

We attribute this slight loss of secure quasar redshifts to the frequency coverage of the Hectospec instrument, which is 3200–9200  $\text{\AA}$ . At this redshift range, the  $H\alpha$  spectral line no longer falls in the Hectospec wavelength coverage, and the fraction of sources with multiple robust line detections results will reduce for all source types. For bright sources with continuum detection in the spectra, the quasars have a relatively featureless continuum whereas the radio galaxies typically have massive old stellar populations with absorption features, potentially leading to the lower success rate for quasars.

We select our sample at low radio frequencies to avoid biases from Doppler boosting of certain components of the radio sources. Doppler boosting would tend to inflate the observed power of a radio source, which could result in a larger sample size, and a higher probability of selecting sources that are not HERGs. However, at low frequencies the total flux density is dominated by the lobes, which are not Doppler boosted. Typical core-dominance values for radio sources with the same type of power as the LOFAR sample (e.g. Baldi et al. 2013) imply that any Doppler boosted components would provide a negligible contribution to our overall sample selection. We are confident that our results are unbiased by not performing any Doppler corrections.

Finally, the largest angular sizes (LAS) of sources in the sample were measured as the diameter of the smallest circle enclosing

**Table 1.** Final sample parameters. LOFAR ID is source\_id in the LOFAR catalogue. RA and Dec. are from the AGES catalogue. Spectral index is given for those sources present in the WSRT catalogue. The classification is as follows: U – unresolved; UE – unresolved but extended morphology; FR II – Fanaroff–Riley II.

LOFAR ID	$z$	Optical RA	Optical Dec.	LAS (arcsec)	LLS (kpc)	Flux density (mJy)	Power (W Hz <sup>-1</sup> )	$\alpha$	Class
Quasars									
909	1.876	219.54611	34.08321	2.4	20.4	494.62 ± 1.9	4.47 ± 0.02 × 10 <sup>27</sup>	-0.53	UE
1105	3.244	219.37666	34.96291	2.6	20.2	9.89 ± 0.3	2.28 ± 0.08 × 10 <sup>26</sup>	-0.50	U
1197	1.485	219.30660	35.09860	6.9	59.6	92.15 ± 0.4	5.43 ± 0.03 × 10 <sup>26</sup>	-0.15	UE
2136	2.187	218.64273	35.16937	2.1	17.9	17.73 ± 0.2	2.10 ± 0.02 × 10 <sup>26</sup>	0.62	U
2988	2.865	218.12744	34.58065	2.3	18.6	8.94 ± 0.3	1.68 ± 0.05 × 10 <sup>26</sup>	-1.27	U
3414	2.049	217.86592	34.62810	3.0	25.6	15.18 ± 0.3	1.60 ± 0.03 × 10 <sup>26</sup>	-0.57	UE
4287	2.352	217.31340	34.63901	2.6	22.0	2.48 ± 0.2	3.34 ± 0.3 × 10 <sup>25</sup>	-1.05	U
4302	2.207	217.29259	35.49635	2.3	19.4	12.78 ± 0.3	1.54 ± 0.03 × 10 <sup>26</sup>	0.29	U
4424	1.036	217.21750	34.86668	2.6	21.6	11.25 ± 0.3	3.33 ± 0.09 × 10 <sup>25</sup>	-0.36	U
4474	0.747	217.17730	35.72420	26.9	202.4	43.74 ± 0.7	6.74 ± 0.1 × 10 <sup>25</sup>		UE
4590	0.413	217.10619	34.92972	28.4	160.3	74.39 ± 0.7	3.40 ± 0.03 × 10 <sup>25</sup>	-0.80	UE/FR II
4769	2.156	216.96770	35.50896	2.5	21.6	5.25 ± 0.2	6.07 ± 0.3 × 10 <sup>25</sup>	-0.59	U
5349	1.255	216.43303	33.92596	25.8	221.0	1651.05 ± 12.8	7.08 ± 0.05 × 10 <sup>27</sup>	-0.73	UE
5426	1.207	216.35101	34.16002	3.4	28.9	15.63 ± 0.4	6.21 ± 0.1 × 10 <sup>25</sup>		U
5442	2.787	216.31882	34.87961	11.1	89.5	188.49 ± 1.0	3.38 ± 0.02 × 10 <sup>27</sup>		UE
5512	1.601	216.23466	35.47827	30.7	266.5	65.32 ± 0.5	4.42 ± 0.03 × 10 <sup>26</sup>		FR II
Radio galaxies									
825	0.439	219.61089	33.84379	79.4	464.6	73.65 ± 0.5	3.82 ± 0.03 × 10 <sup>25</sup>	-0.69	FR II
1093	0.739	219.38063	34.83463	22.6	169.8	87.49 ± 0.5	1.32 ± 0.01 × 10 <sup>26</sup>	-0.53	UE
1148	0.579	219.34889	35.12636	23.8	161.3	107.98 ± 0.6	9.91 ± 0.06 × 10 <sup>25</sup>		UE
1269	2.648	219.21390	33.65285	4.8	39.5	3.79 ± 0.2	6.24 ± 0.4 × 10 <sup>25</sup>	-0.40	UE
1536	0.846	219.01352	33.73015	45.9	361.1	174.87 ± 0.6	3.46 ± 0.01 × 10 <sup>26</sup>	-1.23	FR II
1578	1.132	218.99646	34.75127	18.3	154.2	43.44 ± 0.4	1.53 ± 0.01 × 10 <sup>26</sup>	-0.68	UE
1639	2.117	218.94856	33.88606	5.0	42.8	9.18 ± 0.3	1.03 ± 0.03 × 10 <sup>26</sup>	-0.24	UE
1739	1.290	218.86841	33.32543	10.9	93.5	37.41 ± 0.5	1.69 ± 0.02 × 10 <sup>26</sup>	-0.17	FR II
1758	0.686	218.87160	34.57289	30.8	224.3	147.89 ± 1.2	1.92 ± 0.01 × 10 <sup>26</sup>	-0.50	UE
1823	1.120	218.81210	33.36397	1.7	14.4	25.75 ± 0.4	8.86 ± 0.1 × 10 <sup>25</sup>	-0.78	U
2145	2.464	218.63110	35.01800	13.0	107.5	9.42 ± 0.3	1.37 ± 0.04 × 10 <sup>26</sup>	-0.73	FR II
2406	1.674	218.47987	34.15944	8.8	76.7	11.94 ± 0.3	8.77 ± 0.2 × 10 <sup>25</sup>	-0.56	UE
2493	0.494	218.42067	33.73990	35.5	221.5	61.22 ± 0.4	4.05 ± 0.03 × 10 <sup>25</sup>	-0.62	FR II
2642	0.310	218.31844	34.85692	124.3	583.7	1515.39 ± 1.5	3.82 ± 0.004 × 10 <sup>26</sup>	-0.92	FR II
2643	1.609	218.31567	33.48305	36.7	318.8	32.38 ± 0.4	2.21 ± 0.03 × 10 <sup>26</sup>	-0.63	FR II
2705	0.497	218.29622	33.97461	29.7	186.1	70.08 ± 0.5	4.70 ± 0.03 × 10 <sup>25</sup>	-0.45	UE
2712	2.409	218.29308	33.76791	2.4	19.7	5.12 ± 0.2	7.18 ± 0.3 × 10 <sup>25</sup>	-0.73	U
2720	0.488	218.29130	35.25504	33.1	205.6	186.03 ± 0.9	1.20 ± 0.006 × 10 <sup>26</sup>	-0.76	UE/FR II
2958	0.479	218.14023	33.71775	34.3	210.8	80.30 ± 0.7	4.99 ± 0.04 × 10 <sup>25</sup>	-0.72	UE
2974	2.244	218.13596	33.98435	2.3	19.4	3.59 ± 0.3	4.45 ± 0.3 × 10 <sup>25</sup>	-0.95	U
3278	1.982	217.95490	33.16585	2.9	24.6	5.50 ± 0.4	5.48 ± 0.4 × 10 <sup>25</sup>	-0.39	U
3348	1.775	217.91176	35.59362	1.6	13.9	5.01 ± 0.3	4.10 ± 0.2 × 10 <sup>25</sup>	-0.96	UE
3552	0.863	217.79130	33.88386	7.4	58.2	136.50 ± 1.6	2.81 ± 0.03 × 10 <sup>26</sup>	-0.67	UE
3614	0.726	217.74939	35.36936	90.3	673.6	36.70 ± 0.4	5.34 ± 0.05 × 10 <sup>25</sup>	-0.60	FR II
3631	2.324	217.74316	33.51855	3.2	26.5	7.56 ± 0.2	9.96 ± 0.3 × 10 <sup>25</sup>	-0.98	UE
3671	0.510	217.71825	33.22300	88.2	560.3	654.94 ± 1.5	4.63 ± 0.01 × 10 <sup>26</sup>	-0.73	FR II
3918	1.826	217.54826	35.00576	23.3	201.9	59.28 ± 0.7	5.10 ± 0.06 × 10 <sup>26</sup>	-0.60	FR II
3925	0.778	217.55066	33.24461	35.5	271.8	1014.18 ± 2.9	1.70 ± 0.005 × 10 <sup>27</sup>	-0.76	FR II
3940	3.248	217.53720	34.78715	4.1	31.3	116.00 ± 1.1	2.68 ± 0.02 × 10 <sup>27</sup>	-0.63	U
4058	0.628	217.45322	35.29644	42.6	299.3	53.56 ± 0.4	5.80 ± 0.05 × 10 <sup>25</sup>	-0.63	FR II
4081	1.125	217.42775	33.94859	101.8	857.9	104.62 ± 0.7	3.63 ± 0.03 × 10 <sup>26</sup>	-0.85	FR II
4137	0.656	217.41853	32.96680	64.1	458.7	51.56 ± 0.5	6.11 ± 0.05 × 10 <sup>25</sup>	-0.58	FR II
4294	0.320	217.29977	33.44387	153.2	735.2	302.35 ± 0.7	8.15 ± 0.02 × 10 <sup>25</sup>	-0.95	FR II
4544	2.023	217.14195	34.34181	2.7	23.4	6.44 ± 0.3	6.66 ± 0.3 × 10 <sup>25</sup>		U
4577	0.487	217.12979	33.15258	38.7	239.9	68.24 ± 0.4	4.39 ± 0.03 × 10 <sup>25</sup>	-0.85	FR II
4708	0.868	217.02147	35.22464	5.7	45.1	25.58 ± 0.3	5.33 ± 0.06 × 10 <sup>25</sup>	-0.68	UE/FR II
4831	1.239	216.93529	33.64130	4.2	35.5	22.30 ± 0.4	9.33 ± 0.2 × 10 <sup>25</sup>	-0.16	UE
5037	0.809	216.75853	33.20626	29.3	227.2	34.10 ± 0.4	6.17 ± 0.07 × 10 <sup>25</sup>	-0.58	FR II
5040	0.570	216.75694	33.09038	39.2	263.5	59.51 ± 0.8	5.29 ± 0.07 × 10 <sup>25</sup>		UE
5142	1.351	216.64010	33.53679	29.9	257.8	35.62 ± 0.6	1.76 ± 0.03 × 10 <sup>26</sup>	-0.61	FR II
5171	0.259	216.58580	34.67144	118.1	488.5	352.47 ± 1.3	6.13 ± 0.02 × 10 <sup>25</sup>	-0.63	FR II
5337	0.328	216.42273	34.97419	99.0	483.0	1020.23 ± 5.4	2.89 ± 0.02 × 10 <sup>26</sup>	-0.61	FR II
5374	0.688	216.38220	35.56160	33.1	241.8	42.54 ± 0.5	5.55 ± 0.06 × 10 <sup>25</sup>		UE
5411	1.202	216.38695	33.02372	5.8	49.2	25.96 ± 0.6	1.02 ± 0.02 × 10 <sup>26</sup>		UE

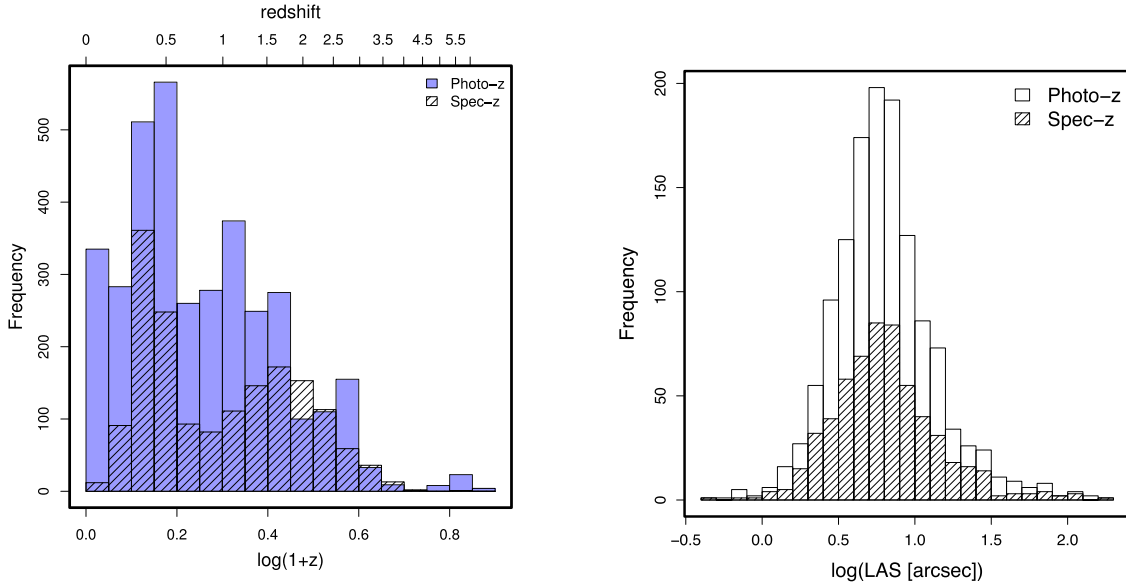


**Figure 1.** Comparison of redshift and radio angular size distributions for AGNs from AGES that have  $I \leq 22.5$  and LOFAR-detected radio emission. Left: distribution of redshifts for sources with photometric redshifts (unfilled histogram) and spectroscopic redshifts (hatched histogram). Right: distribution of radio largest angular size (LAS) for sources with photometric redshifts (unfilled histogram) and spectroscopic redshifts (hatched histogram).

the source at a level of  $5\sigma$  above the local rms. The centre of the circle may or may not correspond to the optical source. The size of a small fraction ( $\sim 5$  per cent) of bent sources may be underestimated since we do not measure along the jets, but this will have a negligible impact on the overall trends. Our results rely on using redshift and LAS to calculate the proper linear size of radio sources. We therefore compare the distributions of the LAS for sources with spectroscopic and photometric redshifts (see right-hand panel of Fig. 1). These distributions are quite similar, indicating that by using only the spectroscopic redshifts we are not missing populations of systematically smaller or larger objects. We therefore do not expect our results to change if the sample were expanded.

### 3 RESULTS

In this section, we present the results from the final LOFAR sample. First, we investigate the projected linear sizes of flat- and steep-spectrum radio sources, without any further knowledge of the type of host galaxy. We then investigate whether the projected linear sizes of quasars and radio galaxies, as identified from the multiwavelength data, are different. This equates to a test of unification through orientation of HERGs. In all cases, we use only the 60 sources with  $P_{150\text{MHz}} \geq 10^{25.5} \text{ W Hz}^{-1}$ .

#### 3.1 Flat- versus steep-spectrum sources

First we test whether there is a systematic difference in projected linear sizes of flat- and steep-spectrum sources. Flat-spectrum sources are likely to be beamed objects with their radio jets close to the line of sight. We use the complementary 1.4 GHz data from a deep Westerbork survey of the Boötes field (de Vries et al. 2002) to calculate the spectral index between 150 MHz and 1.4 GHz. There are 11 flat-spectrum objects with  $\alpha > -0.5$  (18 per cent). The rest of the sources are considered to be steep spectrum and also in the case of no Westerbork detection. Fig. 2 shows the cumulative projected linear sizes of the flat- and steep-spectrum objects and the distribution of sources in the  $P$ - $z$  plane. The average redshifts of the two

types of sources are  $z = 1.23$  for the steep-spectrum sources and  $z = 1.81$  for the flat-spectrum sources. The mean projected linear sizes of the steep- and flat-spectrum sources are  $222.42 \pm 29.81$  and  $50.97 \pm 15.12$  kpc, respectively. The projected linear sizes of steep-spectrum sources are therefore on average  $4.4 \pm 1.4$  times larger than those of the flat-spectrum sources.

For a population of randomly oriented sources, we can calculate the angle (between  $0^\circ$  and  $90^\circ$ ) that would define the division between the two populations. Qualitatively this equates to the probability that a source is oriented such that its jets are within a cone angle of  $\phi$  from the line of sight,  $P(\theta < \phi) = 1 - \cos \phi$ . The relative numbers of flat- and steep-spectrum sources then directly give the angle that divides the two populations. We calculate this angle to be  $\theta_c = 35:3^{+5:2}_{-5:9}$ . The average angles for the steep- and flat-spectrum populations are  $65:9$  and  $24:7$ , respectively. Alternatively, the opening angle can be found from the linear size ratio directly. In this case, we find  $\theta_c = 16:3^{+8:2}_{-4:1}$ , with average angles of  $61:3$  and  $11:5$  for the steep- and flat-spectrum populations, respectively.

#### 3.2 Quasars versus radio galaxies

Next we test whether there is a systematic difference in the projected linear sizes of radio galaxies and quasars. We identify the quasars and radio galaxies using the AGES criteria as described in Section 2.3. The final sample has 44 radio galaxies and 16 quasars above a power cut of  $10^{25.5} \text{ W Hz}^{-1}$ . The cumulative linear sizes and distribution in the  $P$ - $z$  plane are shown in Fig. 3. The radio galaxies have a mean projected linear size of  $232.81 \pm 32.35$  kpc, while the quasars have a mean projected linear size of  $75.97 \pm 21.46$  kpc. This corresponds to the projected linear sizes of radio galaxies being on average  $3.1 \pm 1.0$  times larger than those of quasars. The relative numbers of the sources indicate that the angle of division between the two classes is  $\theta_c = 42:8^{+5:4}_{-6:0}$ . The average angles for the radio galaxy and quasar samples are  $68:5$  and  $29:9$ , respectively. Using the size ratio to calculate the division yields  $23:7^{+13:3}_{-6:1}$ , with average angles for the radio galaxy and quasar samples of  $62:7$  and  $16:7$ , respectively.

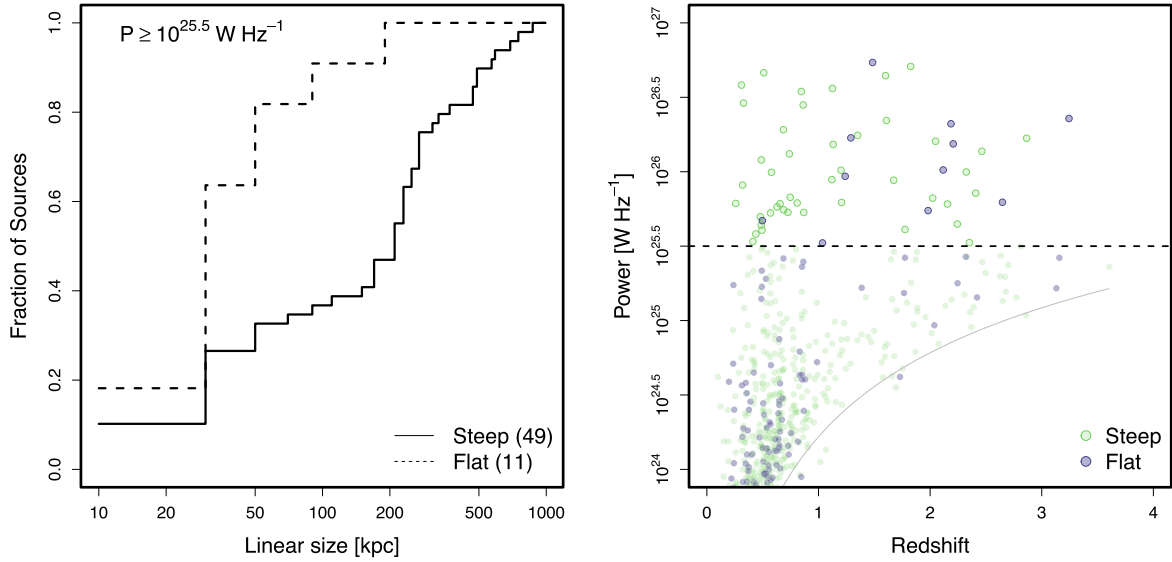


**Figure 2.** Left: cumulative linear sizes for flat- and steep-spectrum radio sources are shown by the solid and dashed lines, respectively. The number of sources in each sample is indicated within parentheses in the legends. Right: the  $P-z$  diagram. The horizontal dashed line indicates the power cut of  $10^{25.5} \text{ W Hz}^{-1}$ . The light grey line shows the flux limit for the survey.

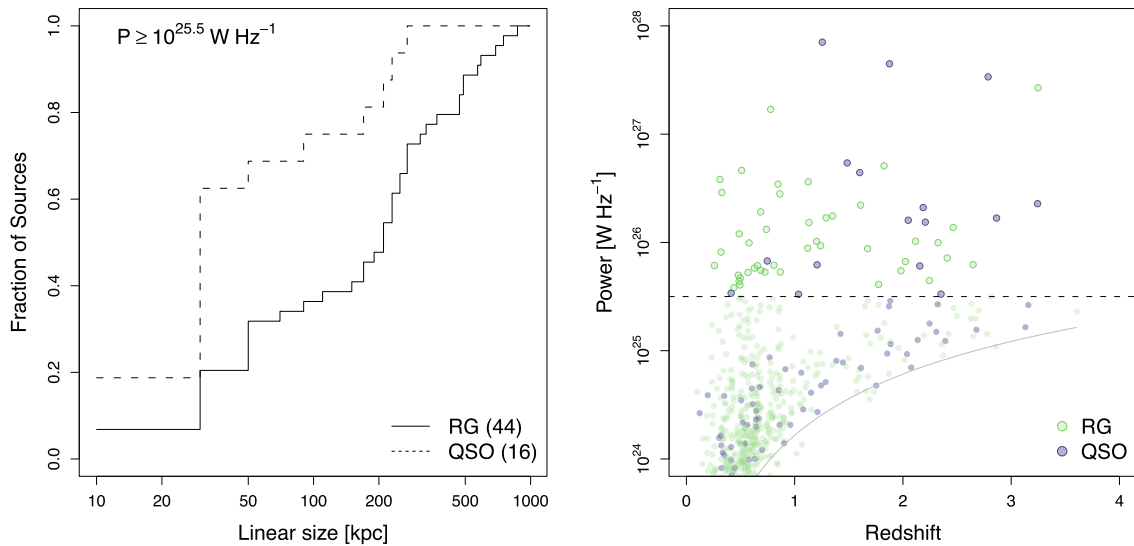


**Figure 3.** Left: cumulative linear sizes for radio galaxies (RG) and quasars (QSO) are shown by the solid and dashed lines, respectively. The number of sources in each sample is indicated within parentheses in the legends. Right: the  $P-z$  diagram. The horizontal dashed line indicates the power cut of  $10^{25.5} \text{ W Hz}^{-1}$ . The light grey line shows the flux limit for the survey.

The average redshifts of the two samples are  $z = 1.16$  and  $1.84$  for radio galaxies and quasars, respectively. A detailed discussion of redshift evolution is deferred to Section 4.2, but here we also report the linear size ratio after correcting the average linear sizes for the two samples to the same average redshift. After this correction, the linear size ratio becomes  $2.0 \pm 0.3$ . The division angle is thus  $39^{\circ}2^{+9.2}_{-6.1}$ , which yields average angles for the radio galaxy and quasar samples of  $67^{\circ}2$  and  $27^{\circ}4$ , respectively.

#### 4 COMBINING LOFAR DATA WITH OTHER SAMPLES

The LOFAR sample of sources comes from an area-limited survey and is missing sources of higher power as these are much rarer. To account for potential radio-power dependencies in the investi-

gation of orientation-based unification theories of radio galaxies and quasars requires the addition of data in other parts of the  $P-z$  plane. In the future, the LOFAR Two-metre Sky Survey (LoTSS; Shimwell et al. 2017) will provide coverage of the entire northern sky, but here we use previous radio surveys to demonstrate what this additional information will provide.

In this section, we briefly describe other low-frequency radio surveys, which cover wider areas to higher flux limits than the LOFAR survey. These surveys are all highly spectroscopically complete, have subsets of quasars already identified and have enough sources for simple binning in redshift. We inspect the cumulative linear sizes of radio galaxies and quasars in these surveys individually, and finally combine the data from our LOFAR survey and several of the previous surveys and investigate trends in projected linear size with power and redshift. Finally, we compare our

**Table 2.** A list of the previous surveys used in this paper. We use the data compiled by Ker et al. (2012) for 7CRS, although the original references are listed in the table. The number of sources given in the table is the number that has been identified as either HERGs (whenever possible) or quasars, and excludes LERGs, FR I sources and those without spectroscopic information.

Survey	Frequency	Flux limit	# Sources	Spectroscopic completeness	HERG/LERG separation	References
3CRR	178 MHz	10.9 Jy	170	100 per cent	Yes	Willott et al. (1999), <sup>a</sup> Grimes et al. (2004)
7CRS	151 MHz	~0.50 Jy	114	92 per cent	Yes	Lacy et al. (1999), Willott et al. (2003), Grimes et al. (2004)
MRC	408 MHz	1 Jy	352	98 per cent	No	Kapahi et al. (1998a,b), Baker et al. (1999)

<sup>a</sup>Available at <http://astroherzberg.org/people/chris-willott/research/3crr/>

observational results with the predictions of an orientation-only unification scenario.

#### 4.1 Other low-frequency samples

The general properties of the previous surveys we use are summarized in Table 2. Briefly, these surveys are the following.

(i) *3CRR* (178 MHz), the revised Third Cambridge Catalogue of Radio Sources. This is the original survey used by Barthel (1989) to show the larger cumulative sizes of radio galaxies when compared to quasars, for the redshift range  $0.5 < z < 1$ . Since then, much more detailed optical information has become available, and the sample is now 100 per cent spectroscopically complete. In addition, near-IR spectroscopy allowed for the identification of HERGs and LERGs, using the equivalent width of [O III] and the ratio of [O II]/[O III] (Willott et al. 1999; Grimes, Rawlings & Willott 2004).

(ii) *7CRS*, the Seventh Cambridge Redshift Survey. This comprises three separate samples (7CI, 7CII, 7CIII) that have been combined. These samples have similar flux limits of 0.51, 0.48 and 0.50 Jy for 7CI, 7CII and 7CIII, respectively. The data for 7CI and 7CII come from Grimes et al. (2004), while the 7CIII data are taken from Lacy et al. (1999). Here we use the compilation from Ker et al. (2012), which has LERG and quasar identifications.

(iii) *MRC* (408 MHz), the Molonglo Radio Catalogue. This survey is complete to 1 Jy with a complete quasar subset identified (Kapahi et al. 1998b; Baker et al. 1999), which we use to identify quasars in the sample. This is the only sample observed at  $\nu > 178$  MHz, and the only sample that does not provide HERG/LERG identification. The inclusion of LERGs may add radio sources with random orientation (i.e. not preferentially in the plane of the sky) to the sample. Since LERGs either lack or have a truncated accretion disc, they are less likely to be classified as quasars and therefore will slightly decrease the average size of radio galaxies.

Overall, these surveys are highly spectroscopically complete (92–100 per cent, see Table 2) and allow for the selection of quasars as a separate class from radio galaxies. With the exception of MRC, the surveys also provide HERG/LERG classification and we are able to remove LERGs from the samples. These surveys occupy space in the  $P$ - $z$  plane that has a range of powers at very low redshifts and a smaller range of higher powers at all redshifts, see Fig. 4.

#### 4.2 Results

We repeat the exercise of calculating the cumulative linear sizes for radio galaxies and quasars for each sample separately. These are shown in Fig. 5 for all samples, with the cumulative linear sizes from the LOFAR sample for comparison. For all samples, we applied the same power cut of  $P > 10^{25.5} \text{ W Hz}^{-1}$ . The LOFAR and

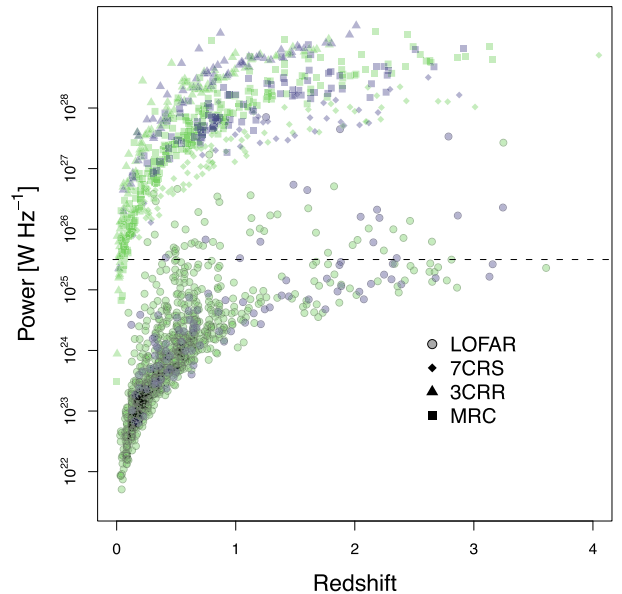


**Figure 4.** Power versus redshift for the three samples described in this section plus the LOFAR sample. Only sources with spectroscopic redshifts are used and above powers of  $P_{150\text{MHz}} > 10^{25.5} \text{ W Hz}^{-1}$  at 150 MHz. Spectral index information was used to convert measured power to  $P_{150\text{MHz}}$  for the MRC and 3CRR samples. Green points represent radio galaxies and purple points represent quasars.

3CRR samples all show cumulative linear sizes of quasars that are smaller than the cumulative linear sizes of radio galaxies. The same is true for 7CRS for almost the entire range of linear sizes. The MRC sample shows that for almost the entire range of linear sizes, quasars and radio galaxies have the same cumulative linear sizes.

As each sample is considered complete by itself, we treat them separately, dividing each sample into low- and high-redshift bins. We determined the dividing redshift for each sample such that about half of the sample lies in each redshift bin but without letting the number of quasars drop below five in a bin. The dividing redshifts used are the following:  $z = 1.5$  (LOFAR),  $z = 0.5$  (3CRR),  $z = 1.5$  (7CRS) and  $z = 1$  (MRC). In each bin, we count the number of radio galaxies and quasars, and measure the mean values of power, redshift and projected linear sizes for each type of source. We calculate the ratio of projected linear sizes of radio galaxies to quasars. The total number of sources in a bin and the number of quasars in that bin are used to calculate the quasar fraction. The uncertainties were determined via standard error propagation methods, except for the case of the quasar fractions for the LOFAR sample, where we used small-number counting uncertainties following the prescription of Gehrels (1986). We assume that the error in spectroscopic redshift is negligible compared to the other measurement errors, and set this to zero.

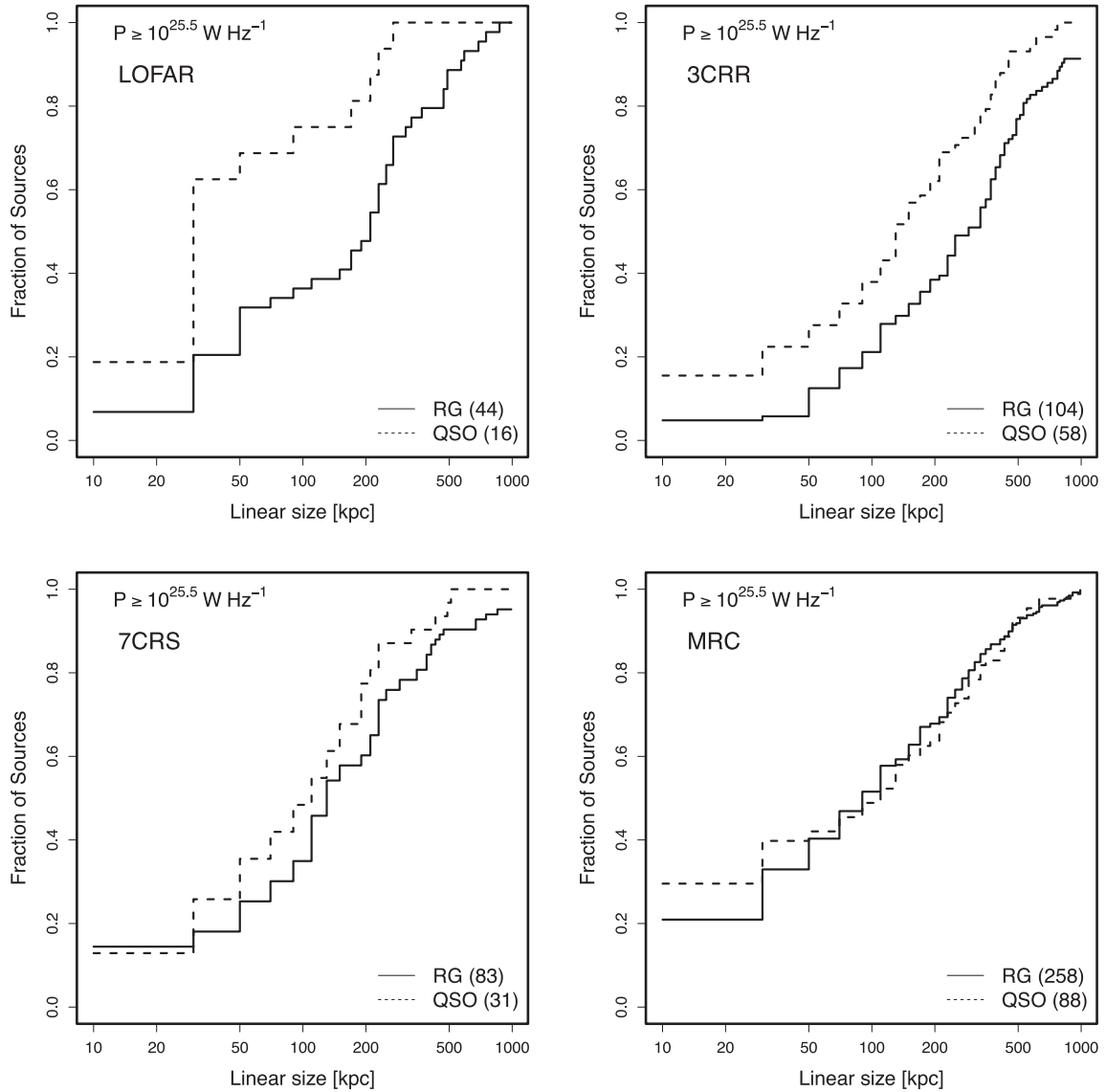


**Figure 5.** The cumulative linear sizes for all samples.

We first examine the measured properties of radio galaxies and quasars by looking at how their projected linear sizes correlate with both power and redshift by using the binned data. This is shown in Fig. 6. There is no clear correlation between projected linear size and power. There does appear to be a correlation between linear size and redshift, with smaller objects found at higher redshifts. The anticorrelation of angular size with redshift is consistent with previous studies (Miley 1968; Wardle & Miley 1974; Neeser et al. 1995; Ker et al. 2012) that also find more compact radio sources at higher redshifts.

To quantify the dependence of size on redshift, we use the same partial rank analysis as described in section 2.3 of Neeser et al. (1995). Assuming a functional form of  $D \propto (1+z)^{-n}$ , where  $D$  is linear size and  $n$  is the ‘evolution strength’, we let  $n$  vary in steps of 0.001 over the range  $0 \leq n \leq 3$ . For each value of  $n$ , we multiplied the source sizes by  $(1+z)^n$  and calculated the partial rank statistic for  $D, z$  given  $P$ . The value of  $n$  that produced a statistic of 0 was taken as the evolution strength, and the upper and lower errors correspond to where the statistic was  $\pm 1$ . We find evolution strengths of  $n = 1.61^{+0.22}_{-0.22}$  for all radio galaxies and quasars considered together,

$n = 1.53^{+0.35}_{-0.35}$  for radio galaxies and  $n = 1.64^{+0.22}_{-0.21}$  for quasars. These values all agree within the uncertainties, indicating that quasars and radio galaxies have the same evolution strength. The values are also in excellent agreement with Neeser et al. (1995), who find an evolution strength for galaxies and quasars of  $n = 1.71^{+0.40}_{-0.48}$  for a flat universe.

We repeat the same exercise but looking at the partial rank statistic for  $D, P$  given  $z$ . Using the functional form  $D \propto P^m$ , we multiply the sources sizes by  $P^{-m}$  and vary  $m$  in steps of  $5 \times 10^{-5}$  from  $-1$  to 1. The values of  $m$  that produce statistics of 0 are consistent with  $m = 0$  for all samples. Specifically, for all sources we find  $m = 1 \pm 3 \times 10^{-5}$ , for radio galaxies we find  $m = 1 \pm 1.5 \times 10^{-4}$  and for quasars we find  $m = 1 \pm 1.5 \times 10^{-5}$ . We therefore conclude that there is no intrinsic relationship between power and size in this sample.

Since an evolution of linear sizes with redshift exists, this could introduce a bias in the projected linear size ratios if the mean redshifts of the radio galaxies and quasars are different. It is possible we could find a larger size ratio of radio galaxy to quasar linear sizes if the radio galaxies tend to be at lower redshifts than the

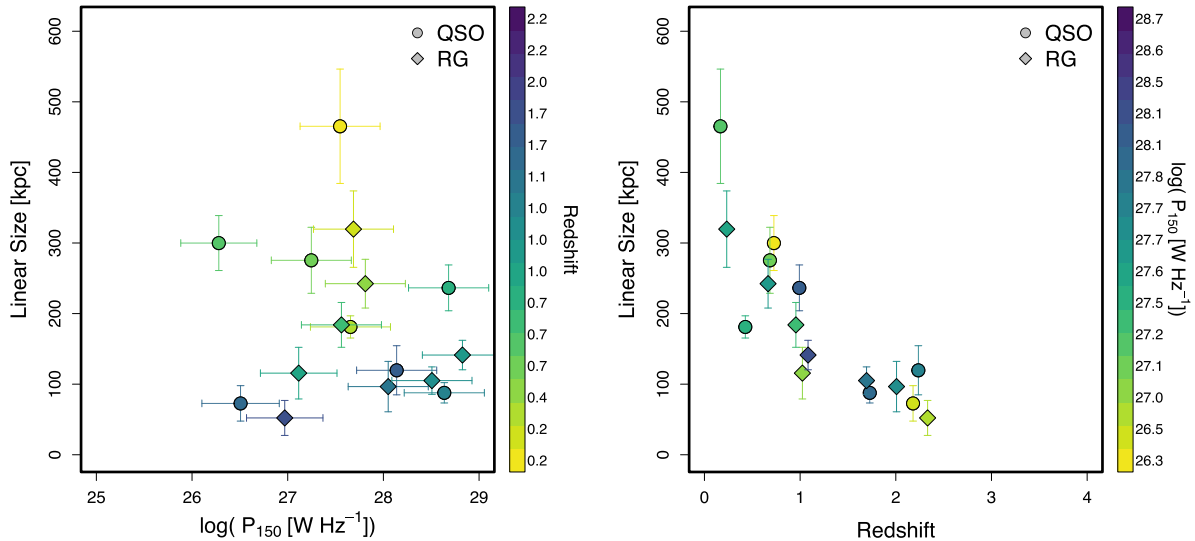


**Figure 6.** The linear sizes of quasars (circles) and radio galaxies (diamonds) plotted against power (left) and redshift (right). The points represent the mean values from the binned data as listed in Table 3. The data are the points coloured according to the colour bar to the right of each plot and show the redshift (left) and power (right).

quasars. We therefore use the evolution strengths calculated above to adjust the average linear sizes of each bin to the same redshift in the following manner:

$$D(z_1) = D(z_2) \frac{(1 + z_1)^{-n}}{(1 + z_2)^{-n}}. \quad (1)$$

This removes the possibility that the results will be biased if the average redshifts for the quasars and radio galaxies are different within a bin. We conservatively do this only for average values within a bin, as the propagation of errors across large redshift ranges will inflate the uncertainties in the linear sizes to be larger than the values themselves if the difference in redshift is too large. Additionally, the fit is not physically motivated and correcting across large redshift ranges is not advisable if, for example, flux limits contribute a significant amount to the redshift evolution of observed size. We correct both the radio galaxy and quasar projected linear sizes to the average redshift of *all* sources in the bin, using the appropriate evolution strength for each sample. The values for average power, linear sizes, along with the number of sources, quasar fraction and radio galaxy to quasar linear size ratio are listed in Table 3. The linear size values are the corrected values, although the average redshift for the individual samples is listed for comparison. Figs 7 and 8 show linear size ratios calculated from the corrected linear sizes.

We also use the redshift evolution to adjust the final results of Section 3.2. This yields a corrected ratio of  $2.0 \pm 0.3$ .

We then investigate how the ratio between radio galaxy and quasar projected linear sizes evolves with power and with redshift, see Fig. 7. The LOFAR, 3CRR and 7CRS samples generally show size ratios larger than unity, while the MRC sample shows size ratios below unity. The errors are large enough that the high-redshift bins for the LOFAR and 7CRS samples could be consistent with unity. There does not appear to be a trend with either power or redshift. This indicates that the linear size ratio remains the same for a large range of powers and out to high redshifts. The fact that the linear size ratio does not clearly evolve with either power or redshift implies that the populations of radio galaxies and quasars *always* have the same relative sizes, regardless of power or redshift evolution.

Lawrence (1991) has proposed that observed increasing quasar fractions with power could arise naturally from a ‘receding torus’ model. In this model, the inner radius of the dusty torus (and hence the opening angle,  $\theta_c$ ) increases as the temperatures achieved via radiation from increasingly powerful AGNs can sublimate dust at larger distances. Using the formulation in section 4.3 of Willott et al. (2000), we can directly relate the predicted linear size ratio to the radio power using the authors’ functional form in equation (1):

$$f_q = 1 - \left( 1 + \frac{P_{150\text{MHz}}}{P_{150\text{MHz}}^*} \tan^2 \theta_0 \right)^{-0.5}, \quad (2)$$

replacing  $L$  with  $P_{150\text{MHz}}$ . We calculate the normalizations,  $P_{150\text{MHz}}^*$  and  $\theta_0$ , from the averages of the power and size ratios given in Table 2. We use the size ratios rather than the quasar fractions to reduce the potential for bias in the quasar fraction (see Section 2.4). The normalization values are  $P_{150\text{MHz}}^* = 1.58 \times 10^{28} \text{ W Hz}^{-1}$  and  $\theta_0 = 62.2^\circ$ . The quasar fractions then directly define the predicted linear size ratios. These are plotted in Fig. 7 (left-hand panel). We also plot the linear size ratios predicted from assuming that the receding torus model does not hold, for two constant opening angles ( $\theta_c = 45^\circ$  and  $60^\circ$ ). Both constant opening angles are consistent within the uncertainties of all data points from the LOFAR, 3CRR and 7CRS samples. The receding torus model describes most of these data points reasonably well and cannot be ruled out. The largest difference between the two models is for lower powers, and future work expanding the LOFAR sample to reduce the uncertainties will be important.

Finally, we investigate how the quasar fraction depends on the radio galaxy to quasar linear size ratio. The results are shown in Fig. 8. For a purely geometric orientation-based unification of radio galaxies and quasars, the observed quasar fraction will define the projected linear size. Apart from the MRC sample and the two low-redshift bins of the 3CRR and 7CRS samples, the data in general are consistent with the theoretical predictions. The predictions assume no intrinsic size distribution, which can artificially inflate the linear size ratio by about 10 per cent (estimated from fig. 3 of DiPompeo et al. 2013). This effect is small compared to the uncertainties we calculate and it is not likely to change our results. The high-redshift

**Table 3.** Calculated values used for comparison of samples. Redshift ranges labelled ‘low’ correspond to sources with redshifts less than or equal to the dividing redshift for each sample (LOFAR:  $z = 1.5$ ; 7CRS:  $z = 1.5$ ; 3CRR:  $z = 0.5$ ; MRC:  $z = 1$ ). The final column ‘Ref.’ refers to the different samples: L = LOFAR; 7 = 7CRS; 3 = 3CRR; M = MRC. Although the average redshifts,  $\bar{z}$ , are given for radio galaxies and quasars, the projected linear sizes (and therefore the ratios) are corrected to the average redshift for *all* sources within a bin, using equation (1).

$z$ bin	$\bar{z}$	Radio galaxies			$\bar{z}$	Quasars			Quasar fraction	Linear size ratio	Ref.
		Power ( $\text{W Hz}^{-1}$ )	Linear size (kpc)	No.		Power ( $\text{W Hz}^{-1}$ )	Linear size (kpc)	No.			
Low	0.726	$1.9 \pm 0.01 \times 10^{26}$	$300 \pm 39$	31	1.02	$1.3 \pm 0.01 \times 10^{27}$	$116 \pm 37$	6	$0.16^{+0.34}_{-0.12}$	$2.59 \pm 0.89$	L
High	2.18	$3.2 \pm 0.05 \times 10^{26}$	$73 \pm 25$	13	2.33	$9.3 \pm 0.07 \times 10^{26}$	$52 \pm 25$	10	$0.43^{+0.88}_{-0.31}$	$1.39 \pm 0.82$	L
Low	0.684	$1.8 \pm 0.18 \times 10^{27}$	$276 \pm 47$	63	0.956	$3.6 \pm 0.36 \times 10^{27}$	$184 \pm 32$	16	$0.20^{+0.41}_{-0.12}$	$1.50 \pm 0.36$	7
High	2.24	$1.4 \pm 0.14 \times 10^{28}$	$120 \pm 35$	20	2.01	$1.1 \pm 0.11 \times 10^{28}$	$97 \pm 36$	15	$0.43^{+0.85}_{-0.28}$	$1.24 \pm 0.58$	7
Low	0.167	$3.5 \pm 0.35 \times 10^{27}$	$465 \pm 81$	67	0.233	$4.9 \pm 0.49 \times 10^{27}$	$320 \pm 54$	18	$0.21^{+0.43}_{-0.12}$	$1.46 \pm 0.35$	3
High	0.992	$4.8 \pm 0.48 \times 10^{28}$	$236 \pm 33$	44	1.08	$6.7 \pm 0.67 \times 10^{28}$	$141 \pm 21$	41	$0.48^{+0.93}_{-0.25}$	$1.67 \pm 0.34$	3
Low	0.427	$4.5 \pm 0.45 \times 10^{27}$	$181 \pm 16$	199	0.665	$6.5 \pm 0.65 \times 10^{27}$	$242 \pm 35$	48	$0.19^{+0.38}_{-0.09}$	$0.75 \pm 0.12$	M
High	1.73	$4.3 \pm 0.43 \times 10^{28}$	$88 \pm 14$	65	1.69	$3.2 \pm 0.32 \times 10^{28}$	$105 \pm 19$	40	$0.38^{+0.74}_{-0.19}$	$0.84 \pm 0.21$	M

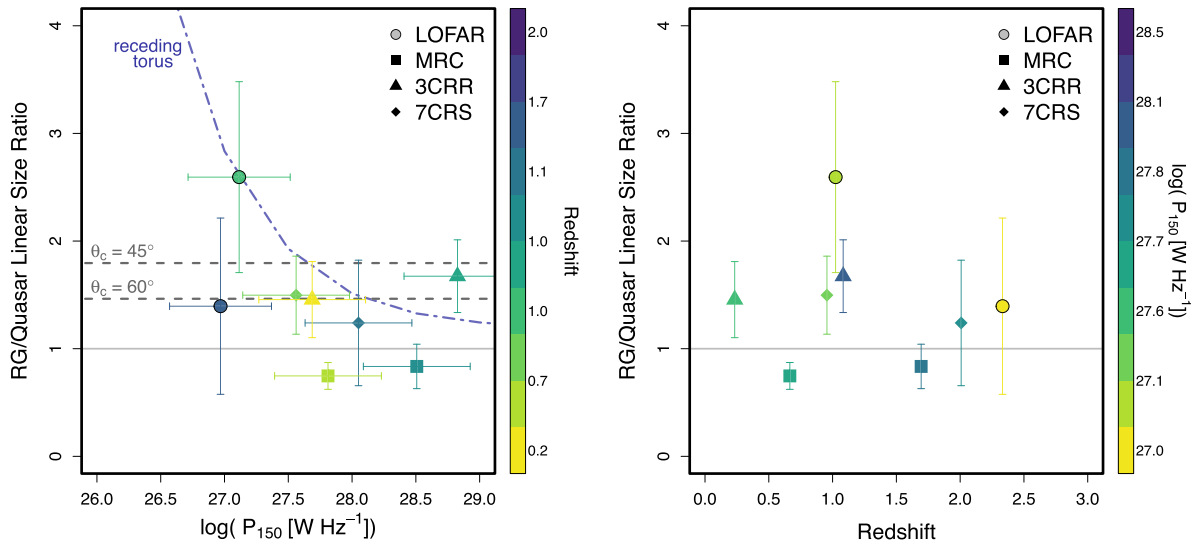


**Figure 7.** The radio galaxy to quasar linear size ratios plotted against power (left) and redshift (right). The symbol shapes represent the sample, with squares for the MRC, triangles for the 3CRR, diamonds for 7CRS and circles for the LOFAR samples. The colour axes are redshift (left) and power (right). The horizontal grey lines indicate where the linear size ratio is unity. The linear size ratio versus power plot also shows theoretical predictions for (i) two constant torus opening angles, shown by the dark grey dashed lines, and (ii) the receding torus model as described in Section 4.2, shown by the blue dash–dotted lines.

LOFAR bin could have a biased quasar fraction as discussed in Section 2.4, but even if the quasar fraction in the high-redshift bin were reduced by a factor of 2 (bringing it in agreement with the low-redshift bin), the data point in Fig. 8 would still be consistent with the theoretical prediction, within the uncertainties.

## 5 DISCUSSION

For the discussion, we first consider how the radio data can be interpreted given an orientation-based unification scenario. We then discuss the possibility that evolution rather than orientation is the dominant effect that explains the data.

### 5.1 Orientation interpretation

First we consider a scheme where the observed fraction of quasars depends *only* on viewing angle, which is supported by other observational evidence. For example, Antonucci & Ulvestad (1985) used high-resolution observations of blazars to show that they are consistent with being normal radio galaxies viewed along the jet axis. Observed differences in depolarization of radio lobes (the

Laing–Garrington effect) also indicate orientation effects, as the approaching (receding) lobe will appear less (more) depolarized due to differential Faraday rotation in the ambient medium along the line of sight (Garrington et al. 1988). In some cases, this can cause sources close to the line of sight (i.e. quasars) to appear one-sided as the receding jet drops below the sensitivity limit. If we assume that all quasars in our LOFAR sample are one-sided and multiply their sizes by a factor of 2 to account for this, we still find a linear size ratio of radio galaxies to quasars of  $1.53 \pm 0.48$ . This is still above unity and therefore consistent with an orientation scheme. This is the *smallest* that the ratio could possibly be, as some quasars have clear double structure.

The unification of HERGs via orientation predicts several key observable characteristics with which we can compare our results. First, the projected linear sizes of quasars should on average be smaller than the projected linear sizes of radio galaxies. The new LOFAR data are consistent with this, as we found a linear size ratio of  $2.0 \pm 0.3$  (for radio galaxies to quasars, after correcting for redshift evolution). For the LOFAR sample, we found a division angle between radio galaxies and quasars of  $39^{\circ}2^{+9}_{-6}$ , which is in agreement with the value of  $44^{\circ}4$  found for the original 3CRR sample

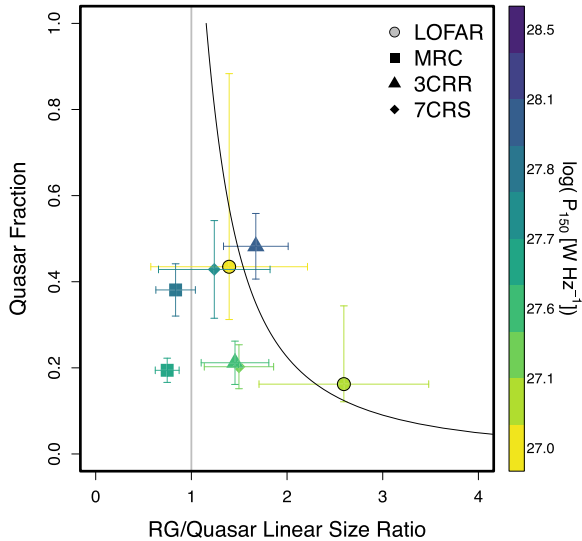


**Figure 8.** The quasar fraction versus radio galaxy to quasar linear size ratio. Each sample is represented by symbols of different shapes as indicated in the legend. The horizontal grey line shows where the ratio between linear sizes of radio galaxies and quasars is unity. The curved black line is the prediction of the relationship between the observed quasar fraction and the projected linear size ratio for a purely geometric orientation-based unification model. The colour axis shows power.

(Barthel 1989; Willott et al. 2000). That would mean that quasars have their radio jets oriented between  $0^\circ$  (line of sight) and  $39^\circ$ , while radio galaxies have jets oriented between  $39^\circ$  and  $90^\circ$  (plane of sky). This is similar to values found from other studies, which use other methods to estimate the critical division angle between quasars and radio galaxies, based on parameters like core dominance or emission line properties. In general, quasars (sometimes called ‘broad-line objects’) have higher values of core dominance, which have been used to estimate division angles of  $50^\circ \pm 5^\circ$  (Baldi et al. 2013),  $60^\circ \pm 10^\circ$  (Marin & Antonucci 2016) or constrained to between  $10^\circ$  and  $80^\circ$  (Aars et al. 2005).

Secondly, beamed radio sources with flat spectra should be oriented close to the line of sight and therefore should also be smaller on average than steep-spectrum sources. The LOFAR data are also consistent with this scenario, and the linear size ratio is  $4.4 \pm 1.4$ , even larger than the linear size ratio for radio galaxies/quasars. The angle of division between flat- and steep-spectrum sources is  $35:3^{+5:2}_{-5:9}$ . This is consistent with the idea that the flux densities of flat-spectrum sources are dominated by beamed radio jets that are oriented close to the line of sight. The fact that this angle is smaller than the division between radio galaxies and quasars is consistent with an orientation-only scheme where there are fewer sources that are beamed than are identified as quasars, if the opening angle of the torus is what determines whether or not a quasar is observed.

Finally, the quasar fraction should be directly correlated with the linear size ratio if *only* orientation is responsible for whether or not we observe a quasar. We find that the LOFAR data are entirely consistent with the predictions (see Fig. 8). The high-redshift bins of both the 7CRS and 3CRR samples are also consistent with this prediction, while the low-redshift bins lie slightly below the prediction. The sizes of the samples limited the analysis to only two redshift bins per sample. With LoTSS, we will be able to fill enough of the  $P$ - $z$  plane to refine the redshift bins and investigate this inconsistency between the low- and high-redshift bins. The MRC sample is not at all consistent with the orientation-only predictions. This is

the only sample of the four we investigated that shows no difference between the sizes of radio galaxies and quasars. Since we treat the samples separately, any systematic offset in size measurements should affect both radio galaxies and quasars in the MRC sample in the same manner, and the *ratio* of the two would still be robust. If there is a population of radio sources that do not participate in the orientation-based unification scheme, the higher selection frequency of the MRC may be impacted to a larger extent than the other surveys. We can find no evidence of this in the available information, but it is possible that the identification and removal of LERGs from the MRC sample could be instructive.

Overall, we find that the LOFAR results are consistent with an orientation-based unification scenario, as are the high-redshift data from the 3CRR and 7CRS samples.

## 5.2 Evolutionary interpretation

Another possibility is that radio galaxies and quasars are linked through an evolutionary scheme rather than by orientation alone. In such a scheme, radio jets would be triggered when quasars become active. The radio jets would grow and finally when the quasar reaches an inactive state the source would be classified as a radio galaxy (still with AGN signatures but lack of emission from an accretion disc). The measured quasar fraction in this case would be interpreted as the fraction of time a source spends as an active quasar, and the linear size ratio would depend on the expansion rate of the radio source. Radio galaxies would be larger than quasars because they are older and have had more time to expand, but this does not account for recurrent quasar activity, as the projected linear size would be correlated with the *first* quasar activity. In the LOFAR sample, the sizes of radio galaxies are on average larger than the sizes of quasars, which is consistent with this evolutionary scheme. However, evolution alone cannot explain observational effects like the Laing–Garrington effect or the presence of scattered quasar light in radio galaxies (e.g. Jackson, Tadhunter & Sparks 1998).

If an evolutionary scheme holds, the fact that higher quasar fractions are seen for the higher redshift bins would mean that either higher redshift sources spend a longer portion of their lives as quasars before becoming radio galaxies or there are simply more young quasars than old radio galaxies at high redshift. If it is true that higher redshift sources spend longer portions of their lives as quasars, the radio jets would have to grow more slowly to be consistent with Fig. 7, where we see no change in the linear size ratio with redshift. Slower growth of radio jets could be due to the higher density ambient medium expected at high redshift, but it would not change the amount of time that a quasar is active. If there are simply more young quasars at higher redshift, we would expect to see an evolution with redshift of the linear size ratios between quasars and radio galaxies, which we do not observe. This could possibly be rectified if *all* sources (quasars and radio galaxies) at high redshift were younger than those at low redshift. Of course evolutionary effects will play a role – but apparently not a dominant one.

## 6 CONCLUSIONS

In this paper, we used a new LOFAR survey of the Boötes field to show that the projected linear sizes of steep-spectrum radio sources are on average  $4.4 \pm 1.4$  times larger than those of flat-spectrum radio sources. This is consistent with an orientation scheme for radio jets, where beamed flat-spectrum radio sources lie closer to the line of sight and therefore have smaller projected sizes.

We have also shown that for radio galaxies and quasars in the LOFAR survey, as identified by AGES criteria, the projected linear sizes of radio galaxies are on average  $3.1 \pm 1.0$  times larger than those of quasars, which becomes  $2.0 \pm 0.3$  after correcting for the redshift evolution of linear sizes. This is also consistent with an orientation-based unification scheme, where the presence of a dusty obscuring torus prevents the identification of a quasar unless the radio jets are preferentially aligned closer to the line of sight.

When combining the new LOFAR measurements with previous surveys and separating each sample into low- and high-redshift bins, we find no clear trend between the linear size ratio of radio galaxies to quasars and redshift or power. The lack of a clear trend between the linear size ratio and redshift suggests that the populations of radio galaxies and quasars *always* have the same sizes relative to each other. The lack of a trend with redshift is consistent with orientation, or else an evolutionary scheme where the sizes of radio galaxies and quasars are evolving in exactly the same manner at exactly the same rate.

When comparing theoretical predictions of orientation-based unification models for the relation between quasar fraction and linear size ratio to the observations, the LOFAR data are consistent with the predictions. Other low-frequency surveys are in agreement for their high-redshift bins, while the MRC sample, which is measured at a higher frequency, consistently shows that quasars are on average larger than radio galaxies. The comparison between the linear size ratios and power shows that the data (aside from the MRC sample) are consistent with a constant opening angle for sources of all powers, but the ‘receding torus’ model cannot be ruled out at the present time. The largest difference between the models is for lower power sources, and expanding the LOFAR sample to reduce the uncertainties will be crucial to distinguishing between these two models.

Ultimately the LOFAR Tier 1 survey will cover the northern sky above declination  $0^\circ$ , providing millions of radio sources. Spectroscopic redshifts and host galaxy identifications will be provided by a survey with the WEAVE that goes online 2018 March. The WEAVE–LOFAR survey (Smith 2016) is dedicated to providing this information for  $\sim 10^6$  LOFAR-detected sources in the Tier 1 survey. With this information, and updated theoretical models that allow us to account for intrinsic size distributions (Saxena et al., 2017), we will be able to break the degeneracy between orientation and evolutionary effects in unification schemes.

## ACKNOWLEDGEMENTS

We thank the anonymous referee for useful comments on the manuscript. LKM acknowledges financial support from NWO Top LOFAR project, project no. 614.001.006. WLW acknowledges support from the UK Science and Technology Facilities Council [ST/M001008/1]. PNB is grateful for support from the UK STFC via grant ST/M001229/1. MJJ acknowledges support from UK Science and Technology Facilities Council and the South African SKA Project. EKM acknowledges support from the Australian Research Council Centre of Excellence for All-sky Astrophysics (CAASTRO) through project number CE110001020. HJAR and KJD acknowledge support from the ERC Advanced Investigator programme NewClusters 321271.

## REFERENCES

Aars C. E., Hough D. H., Yu L. H., Linick J. P., Beyer P. J., Vermeulen R. C., Readhead A. C. S., 2005, *AJ*, 130, 23

- Antonucci R. R. J., 1982, *Nature*, 299, 605  
 Antonucci R. R. J., 1984, *ApJ*, 278, 499  
 Antonucci R., 1993, *ARA&A*, 31, 473  
 Antonucci R. R. J., Ulvestad J. S., 1985, *ApJ*, 294, 158  
 Baker J. C., Hunstead R. W., Kapahi V. K., Subrahmanya C. R., 1999, *ApJS*, 122, 29  
 Baldi R. D., Capetti A., Buttiglione S., Chiaberge M., Celotti A., 2013, *A&A*, 560, A81  
 Barthel P. D., 1989, *ApJ*, 336, 606  
 Barthel P. D., Hooimeyer J. R., Schilizzi R. T., Miley G. K., Preuss E., 1989, *ApJ*, 336, 601  
 Best P. N., Heckman T. M., 2012, *MNRAS*, 421, 1569  
 Best P. N., Röttgering H. J. A., Lehnert M. D., 1999, *MNRAS*, 310, 223  
 Brammer G. B., van Dokkum P. G., Coppi P., 2008, *ApJ*, 686, 1503  
 Brown M. J. I., Dey A., Jannuzi B. T., Brand K., Benson A. J., Brodwin M., Croton D. J., Eisenhardt P. R., 2007, *ApJ*, 654, 858  
 Brown M. J. I. et al., 2008, *ApJ*, 682, 937  
 Brown M. J. I. et al., 2014, *ApJS*, 212, 18  
 Cohen M. H., Ogle P. M., Tran H. D., Goodrich R. W., Miller J. S., 1999, *AJ*, 118, 1963  
 de Vries W. H., Morganti R., Röttgering H. J. A., Vermeulen R., van Breugel W., Rengelink R., Jarvis M. J., 2002, *AJ*, 123, 1784  
 DiPompeo M. A., Runnoe J. C., Myers A. D., Boroson T. A., 2013, *ApJ*, 774, 24  
 Evans D. A., Worrall D. M., Hardcastle M. J., Kraft R. P., Birkinshaw M., 2006, *ApJ*, 642, 96  
 Fanaroff B. L., Riley J. M., 1974, *MNRAS*, 167, 31p  
 Garrington S. T., Leahy J. P., Conway R. G., Laing R. A., 1988, *Nature*, 331, 147  
 Gehrels N., 1986, *ApJ*, 303, 336  
 Grimes J. A., Rawlings S., Willott C. J., 2004, *MNRAS*, 349, 503  
 Hardcastle M. J., Evans D. A., Croston J. H., 2006, *MNRAS*, 370, 1893  
 Hardcastle M. J., Evans D. A., Croston J. H., 2007, *MNRAS*, 376, 1849  
 Ho L. C., 2008, *ARA&A*, 46, 475  
 Jackson N., Tadhunter C., Sparks W. B., 1998, *MNRAS*, 301, 131  
 Jannuzi B. T., Dey A., 1999, in Bunker A. J., van Breugel W. J. M., eds, *ASP Conf. Ser. Vol. 193, The Hy-Redshift Universe: Galaxy Formation and Evolution at High Redshift*. Astron. Soc. Pac., San Francisco, p. 258  
 Janssen R., 2017, PhD thesis, Leiden University  
 Kapahi V. K., Athreya R. M., van Breugel W., McCarthy P. J., Subrahmanya C. R., 1998a, *ApJS*, 118, 275  
 Kapahi V. K., Athreya R. M., Subrahmanya C. R., Baker J. C., Hunstead R. W., McCarthy P. J., van Breugel W., 1998b, *ApJS*, 118, 327  
 Ker L. M., Best P. N., Rigby E. E., Röttgering H. J. A., Gendre M. A., 2012, *MNRAS*, 420, 2644  
 Kochanek C. S. et al., 2012, *ApJS*, 200, 8 (K12)  
 Lacy M., Rawlings S., Hill G. J., Bunker A. J., Ridgway S. E., Stern D., 1999, *MNRAS*, 308, 1096  
 Laing R. A., Riley J. M., Longair M. S., 1983, *MNRAS*, 204, 151  
 Larson R. B., 2010, *Nat. Phys.*, 6, 96  
 Lawrence A., 1991, *MNRAS*, 252, 586  
 Marin F., Antonucci R., 2016, *ApJ*, 830, 82  
 Miley G. K., 1968, *Nature*, 218, 933  
 Narayan R., Yi I., 1994, *ApJ*, 428, L13  
 Neeser M. J., Eales S. A., Law-Green J. D., Leahy J. P., Rawlings S., 1995, *ApJ*, 451, 76  
 Ogle P. M., Cohen M. H., Miller J. S., Tran H. D., Fosbury R. A. E., Goodrich R. W., 1997, *ApJ*, 482, L37  
 Ogle P., Whyson D., Antonucci R., 2006, *ApJ*, 647, 161  
 Planck Collaboration XIII, 2016, *A&A*, 594, A13  
 Polletta M. et al., 2007, *ApJ*, 663, 81  
 Quataert E., 2001, in Peterson B. M., Pogge R. W., Polidan R. S., eds, *ASP Conf. Ser. Vol. 224, Probing the Physics of Active Galactic Nuclei*. Astron. Soc. Pac., San Francisco, p. 71  
 Rigby E. E., Best P. N., Brookes M. H., Peacock J. A., Dunlop J. S., Röttgering H. J. A., Wall J. V., Ker L., 2011, *MNRAS*, 416, 1900  
 Rigby E. E., Argyle J., Best P. N., Rosario D., Röttgering H. J. A., 2015, *A&A*, 581, A96

- Saxena A., Röttgering H. J. A., Rigby E. E., 2017, MNRAS, in press  
Schmidt G. D., Smith P. S., 2000, ApJ, 545, 117  
Shakura N. I., Sunyaev R. A., 1973, A&A, 24, 337  
Shimwell T. W. et al., 2017, A&A, 598, A104  
Singal A. K., 2014, AJ, 148, 16  
Singal A. K., Singh R. L., 2013, MNRAS, 435, L38  
Smith D. J. B., 2016, in Skillen I., Barcells M., Trager S., eds, ASP Conf. Ser. Vol. 507, Multi-Object Spectroscopy in the Next Decade: Big Questions, Large Surveys, and Wide Fields. Astron. Soc. Pac., San Francisco, p. 373  
Stern D. et al., 2005, ApJ, 631, 163  
Tasse C., Best P. N., Röttgering H., Le Borgne D., 2008, A&A, 490, 893  
Urry C. M., Padovani P., 1995, PASP, 107, 803  
van der Wolk G., Barthel P. D., Peletier R. F., Pel J. W., 2010, A&A, 511, A64  
van Haarlem M. P. et al., 2013, A&A, 556, A2  
Wardle J. F. C., Miley G. K., 1974, A&A, 30, 305  
Whysong D., Antonucci R., 2004, ApJ, 602, 116  
Williams W. L. et al., 2016, MNRAS, 460, 2385  
Williams W. L. et al., 2017, MNRAS, in press  
Willott C. J., Rawlings S., Blundell K. M., Lacy M., 1999, MNRAS, 309, 1017  
Willott C. J., Rawlings S., Blundell K. M., Lacy M., 2000, MNRAS, 316, 449  
Willott C. J., Rawlings S., Jarvis M. J., Blundell K. M., 2003, MNRAS, 339, 173

This paper has been typeset from a  $\text{\TeX}/\text{\LaTeX}$  file prepared by the author.